Branching fractions and polarizations of $D \to V\ell\nu_\ell$ within QCD light-cone sum rule

Hai-Bing Fu,[1] Wei Cheng ⊙,[2,3,*] Long Zeng,[1] Dan-Dan Hu,[1] and Tao Zhong[1]

[1]*Institute of Particle Physics and Department of Physics, Guizhou Minzu University, Guiyang 550025, People's Republic of China*

[2]*CAS Key Laboratory of Theoretical Physics, Institute of Theoretical Physics, Chinese Academy of Sciences,*
Beijing 100190, People's Republic of China

[3]*Institute of Theoretical Physics, Chinese Academy of Sciences, P.O. Box 2735, Beijing 100190, People's Republic of China*

In this paper, we make a detailed study of the $D \to V$ helicity form factors (HFFs) within the framework of the QCD light-cone sum rule (LCSR) up to twist-4 accuracy. After extrapolating the LCSR predictions of HFFs to the whole physical q^2 region, we get the longitudinal, transverse, and total $|V_{cq}|$-independent decay widths of semileptonic decay $D \to V\ell^+\nu_\ell$. Meanwhile, the branching fractions of these decays are also obtained by using the $D^0(D^+)$-meson lifetime, which agrees well with the BESIII results within the error bars. As a further step, we also investigate the differential and mean predictions for charged lepton (vector meson) polarization in the final state $P_{\mathrm{L,T}}^\ell$ ($F_{\mathrm{L,T}}^\ell$), the forward-backward asymmetry $\mathcal{A}_{\mathrm{FB}}^\ell$, and the lepton-side convexity parameters $\mathcal{C}_{\mathrm{F}}^\ell$. Our predictions are consistent with covariant confining quark model results within errors. Thus, we think the LCSR approach for HFFs is applicable for dealing with the D-meson semileptonic decays.

I. INTRODUCTION

Semileptonic decays of charm mesons to vector mesons are a significant component in deeper understanding of the standard model (SM) in the post-Higgs era. Those decays not only are directly related to Cabibbo Kobayashi Maskawa (CKM) matrix elements providing a window to study the *CP*-violation problem [1–8] but also contain the flavor-changing neutral current (FCNC) processes, which are sensitive to new physics (NP) because it occurs in at least one loop level in the SM [9–13]. For the *D*-meson semileptonic decay processes, the BESIII [14–16] and CLEO [17–22] Collaborations have reported the branching fraction and form factors at a large recoil point. In 2019, the BESIII Collaboration measured the $D \to \rho\ell\nu_\ell$ branching fraction, i.e., $\mathcal{B}(D^0 \to \rho^-e^+\nu_e) = (1.445 \pm 0.058_{\mathrm{stat}} \pm 0.039_{\mathrm{syst}}) \times 10^{-3}$ and $\mathcal{B}(D^+ \to \rho^0e^+\nu_e) = (1.860 \pm 0.070_{\mathrm{stat}} \pm 0.061_{\mathrm{syst}}) \times 10^{-3}$ [23]; meanwhile, they also presented an improved measurement for the $D \to K^*(892)^-e^+\nu_e$ branching fraction, i.e., $\mathcal{B}(D^0 \to K^*(892)^-e^+\nu_e) = (2.033 \pm 0.046_{\mathrm{stat}} \pm 0.047_{\mathrm{syst}}) \times 10^{-2}$ [24] in the same year. It is worth noting that BESIII recently published their first measurements for the $D^+ \to \omega\mu^+\nu_\mu$ branching fraction in 2020, i.e., $\mathcal{B}(D^+ \to \omega\mu^+\nu_\mu) = (17.7 \pm 1.8_{\mathrm{stat}} \pm 1.1_{\mathrm{syst}}) \times 10^{-4}$, which is realized by applying an e^+e^- collision data sample corresponding to an integrated luminosity of 2.93 fb^{-1} collected with the BESIII detector at a center-of-mass energy of 3.773 GeV [25].

To further the understanding of the $D \to V$ semileptonic decay processes, the complete angular distribution and polarization information should be investigated, such as the longitudinal and transverse polarizations of the final charged lepton $P_{\mathrm{L,T}}^\ell(q^2)$ and the final vector meson $F_{\mathrm{L,T}}^\ell(q^2)$, the forward-backward asymmetry $\mathcal{A}_{\mathrm{FB}}^\ell(q^2)$, and the lepton-side convexity parameter $\mathcal{C}_{\mathrm{F}}^\ell(q^2)$. On the one hand, there is little theoretical research on that polarization information and even less experimental research, but one can find numerous experimental and theoretical studies for that of the B meson [26–35]. On the other hand, the QCD light-cone sum rule (LCSR) is an effective method to study the heavy meson to light meson decay processes that are actually an FCNC process of the heavy quark to light quark transition. The $D \to V$ decay corresponds to the transition of a heavy quark to a light quark $c \to q(u, d, s)$, and the mass of the charm quark is of the order of 1 GeV, which indicate the LCSR is applicable in studying the $D \to V$ decay process. Therefore, in this paper, we will study those observations for the semileptonic $D \to V\ell^+\nu_\ell$ decays within the framework of the LCSR.

The LCSR is an important method in dealing with the semileptonic decays [36–45]. Its main strategy is to construct an analytic heavy-to-light correlator function in the whole q^2 region and then make an operator product expansion (OPE) and a hadron expression for it in the spacelike and timelike regions, respectively, finally combining the results achieved in those two ways to get the form factors with the help of Borel transformation. Both transition form factors (TFFs) and helicity form factors (HFFs) contain information on meson semileptonic decays independently because they can describe the nonperturbative hadronic matrix elements of meson semileptonic decays independently. One can decompose the hadronic matrix elements by applying the momentum of initial and final meson states to obtain TFFs [46–53], which will lead to a mix of longitudinal and transverse polarizations

TABLE I. Resonance masses of quantum number J^P that are indicated as being necessary for the parametrization of $D \to V$ HFFs $\mathcal{D}_{V,\sigma}$ [57,58] with $\sigma = 0, 1, 2, t$.

F_i	J^P	$m_{R,i}$ (GeV)
$\mathcal{D}_{V,t}$	0^-	1.864
$\mathcal{D}_{V,0;2}$	1^+	2.420
$\mathcal{D}_{V,1}$	1^-	2.007

of the meson among those TFFs. Thus, TFFs cannot express the polarization information of meson decay accurately.

The HFFs opened a new avenue to deal with those matrix elements [54–56]. HFFs decompose it by applying the off-shell W-boson polarization vectors, which leads to a good polarization property, i.e., research on tracking polarization. Specifically, the longitudinal and transverse decay information can be completely separated, which is very useful for probing the longitudinal and transverse polarizations separately. Especially, both the decay widths of D-meson longitudinal and transverse components contain the usual TFF [$A_1(q^2)$], which means D-meson longitudinal and transverse components are related to each other. However, in the case of HFFs, the decay widths of the D-meson longitudinal (transverse) component are related to the $\mathcal{D}_{V,0}(q^2)$ [$\mathcal{D}_{V,1}(q^2)$, $\mathcal{D}_{V,2}(q^2)$] HFF, which means the decay widths of the D-meson longitudinal and transverse components are separated completely and have no influence on each other. In addition, HFF also enjoys some other advantages, such as dispersive bounds on the HFF parametrization and direct relations between the HFFs and the spin-parity quantum numbers (Table I). For a more detailed discussion, one can refer to the literature [54–56].

The remaining parts of this paper are organized as follows. In Sec. II, we introduce the physical observable for $D \to V(\rho, \omega, K^*)\ell^+\nu_\ell$ semileptonic decay processes and calculate the HFFs within the LCSR approach. In Sec. III, after fixing the hadron input parameters for HFFs and extrapolating those HFFs to the whole q^2 region with simplified series expansion (SSE), we then apply it to investigate the $D \to V$ semileptonic decay observables, such as the decay width, branching fraction, and polarizations, and also compare our results with available experimental and other theoretical predictions. Finally, we briefly summarize in Sec. IV.

II. CALCULATION TECHNOLOGY

A. $D \to V\ell^+\nu_\ell$ semileptonic decays

The $D \to V\ell^+\nu_\ell$ semileptonic decay process is displayed in Fig. 1. The corresponding invariant matrix element can be expressed as follows:

$$\mathcal{M}(D \to V\ell^+\nu_\ell) = \frac{G_F}{\sqrt{2}}V_{cq}^*H^\mu L_\mu, \quad (1)$$

where the Fermi constant $G_F = 1.166 \times 10^{-5}\,\text{GeV}^{-2}$, leptonic current $L_\mu = \bar{v}_\ell\gamma_\mu(1-\gamma_5)\ell$, and the hadron matric element $H^\mu = \langle V|V^\mu - A^\mu|D\rangle$, with flavor-changing vector current $V^\mu = \bar{q}\gamma^\mu c$ and axial-vector current $A^\mu = \bar{q}\gamma^\mu\gamma_5 c$.
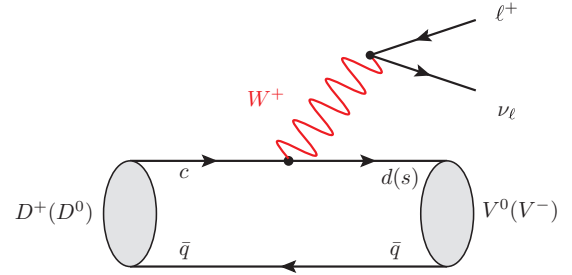

FIG. 1. Typical diagram for the $D \to V\ell^+\nu_\ell$ semileptonic decay, where $q = u, d$ and $V = \rho, \omega, K^*$ mesons.

To get accurate polarization properties of the semileptonic decay $D \to V\ell^+\nu_\ell$, one can decompose the hadron matric element H^μ into the HFFs by the off-shell W-boson polarization vectors. Specifically speaking,

$$\mathcal{D}_{V,\sigma}(q^2) = \sqrt{\frac{q^2}{\lambda}}\sum_{\alpha=0,\pm,t}\epsilon_\sigma^{*\mu}(q)\langle V(\tilde{p},\tilde{\epsilon}_\alpha)|\bar{q}\gamma_\mu(1-\gamma^5)c|D(p)\rangle,$$

$$(2)$$

where the standard kinematic function is $\lambda = (t_- - q^2)(t_+ - q^2)$, with $t_\pm = (m_D \pm m_V)^2$ and $\epsilon_\sigma^{*\mu}(q)$ representing transverse ($\sigma = \pm$), longitudinal ($\sigma = 0$), and timelike ($\sigma = t$) polarization vectors. For the convenience of polarization research, two HFFs, $\mathcal{D}_{V,(1,2)}(q^2)$, are defined by a linear combination of the transverse helicity projection vector, i.e., $\epsilon_{(1,2)}(q) = [\epsilon_-(q) \mp \epsilon_+(q)]/\sqrt{2}$, which will be discussed in the following section.

The polar angle differential decay distribution in the momentum transfer squared, defined by the angle between $\vec{q} = \vec{p}_D - \vec{p}_V$ and the three-momentum of the charged lepton in the rest frame, can be written as follows:

$$\frac{d^2\Gamma}{dq^2d\cos\theta} = \frac{|\mathbf{p_V}|v}{(2\pi)^3 32m_D^2}\sum_{\text{pol}}|\mathcal{M}|^2, \quad (3)$$

where $|\mathbf{p_V}| = \lambda^{1/2}/(2m_D^2)$, $v = (1 - m_\ell^2/q^2)$, and the covariant contraction $\sum_{\text{pol}}|\mathcal{M}|^2$ can be converted to a sum of bilinear products of hadronic HFFs and leptonic helicity amplitude by applying the completeness relation to the polarization four-vectors of the process. So the total differential decay width of $D \to V\ell\nu_\ell$ can be expressed as

$$\frac{1}{|V_{cq}|^2}\frac{d\Gamma}{dq^2} = \mathcal{G}\lambda^{3/2}v^2\left[(1+\delta_\ell)\sum\mathcal{D}_{V,i}^2(q^2) + 3\delta_\ell\mathcal{D}_{V,t}^2(q^2)\right]$$

$$= \mathcal{G}\lambda^{3/2}v^2\mathcal{D}_{\text{tot}}^2(q^2), \quad (4)$$

with $\delta_\ell = m_\ell^2/(2q^2)$, $\mathcal{G} = G_F^2/(192\pi^3 m_D^3)$, and variable $i = 0, 1, 2$. The detailed expression reads

$$\sum\mathcal{D}_{V,i}^2 = \mathcal{D}_{V,0}^2 + \mathcal{D}_{V,1}^2 + \mathcal{D}_{V,2}^2. \quad (5)$$

As we know, the total decay width can be separated into longitudinal and transverse parts, i.e., $\Gamma = \Gamma^L + \Gamma^T$. The decay width for the vector meson longitudinal component Γ^L is defined as

$$\Gamma^L(q^2) = \mathcal{G}|V_{cq}|^2\int_0^{q^2_{\text{max}}}dq^2\lambda(q^2)^{3/2}\mathcal{D}_{V,0}^2(q^2), \quad (6)$$

and the decay width for the vector meson transverse component Γ^{T} is defined as

$$\Gamma^{\mathrm{T}}(q^2) = \mathcal{G}|V_{cq}|^2 \int_0^{q^2_{\max}} dq^2 \lambda(q^2)^{3/2} \sum \mathcal{D}^2_{V,j}, \tag{7}$$

where the variable j is the summation index, $j = 1, 2$.

For the polarization properties of the semileptonic decay $D \to V\ell^+\nu_\ell$, one can study the longitudinal and transverse polarizations first. Specifically, with the help of HFFs, the longitudinal P^ℓ_{L} and transverse P^ℓ_{T} polarizations of the charged lepton in the final state and the longitudinal F^ℓ_{L} and transverse F^ℓ_{T} polarization fractions of the vector meson in the final state are given by

$$P^\ell_{\mathrm{L}} = 1 - \frac{2\sum \mathcal{D}^2_{V,i}}{\mathcal{D}_{\mathrm{tot}}}, \quad P^\ell_{\mathrm{T}} = \frac{3\pi\sqrt{\delta_\ell}}{2\sqrt{2}}\frac{\mathcal{D}_{V,1}\mathcal{D}_{V,2} - \mathcal{D}_{V,0}\mathcal{D}_{V,t}}{\mathcal{D}_{\mathrm{tot}}}, \quad F^\ell_{\mathrm{L}} = \frac{3\mathcal{D}^2_{V,t}\delta_\ell + (1 + \delta_\ell)\mathcal{D}^2_{V,0}}{\mathcal{D}_{\mathrm{tot}}}, \quad F^\ell_{\mathrm{T}} = \frac{(1 + \delta_\ell)(\mathcal{D}^2_{V,1} + \mathcal{D}^2_{V,2})}{\mathcal{D}_{\mathrm{tot}}}. \tag{8}$$

And the forward-backward asymmetry $\mathcal{A}^\ell_{\mathrm{FB}}$ can be written as

$$\mathcal{A}^\ell_{\mathrm{FB}} = \frac{d\Gamma(F) - d\Gamma(B)}{d\Gamma(F) + d\Gamma(B)} = \frac{\int_0^1 d\cos\theta \, d\Gamma/d\cos\theta - \int_{-1}^0 d\cos\theta \, d\Gamma/d\cos\theta}{\int_0^1 d\cos\theta \, d\Gamma/d\cos\theta + \int_{-1}^0 d\cos\theta \, d\Gamma/d\cos\theta} = \frac{3}{2}\frac{2\delta_\ell\mathcal{D}_{V,0}\mathcal{D}_{V,t} - \mathcal{D}_{V,1}\mathcal{D}_{V,2}}{(1 + \delta_\ell)\sum \mathcal{D}^2_{V,i} + \delta_\ell\mathcal{D}^2_{V,t}}. \tag{9}$$

The lepton-side $\mathcal{C}^\ell_{\mathrm{F}}$ convexity parameters has the form

$$\mathcal{C}^\ell_{\mathrm{F}} = -\frac{3}{4}\frac{(2\mathcal{D}^2_{V,0} - \mathcal{D}^2_{V,1} - \mathcal{D}^2_{V,2})(1 - 2\delta_\ell)}{\mathcal{D}_{\mathrm{tot}}}. \tag{10}$$

In order to make a comparison with other approaches, we take the same approach as [59] to deal with the q^2 average of those observables. Specifically, if an observable A has the form $A = \mathcal{D}_x/\mathcal{D}_y$, one can multiply both the numerator and denominator by the phase-space factor and then integrate the two separately. The detailed expression can be written as

$$\langle A \rangle = \frac{\int C(q^2)\mathcal{D}_x dq^2}{\int C(q^2)\mathcal{D}_y dq^2}, \tag{11}$$

with the q^2 dependence phase-space factor

$$C(q^2) = |\mathbf{p_V}|\frac{(q^2 - m^2_\ell)^2}{q^2}. \tag{12}$$

B. The $D \to V$ HFFs

To derive LCSRs for the four HFFs, i.e., $\mathcal{D}_{V,\sigma}(q^2)$ with $\sigma = 0, 1, 2, t$, we first structure a two-point correlation function according to LCSR strategy as follows:

$$\Pi_\sigma(p, q) = i\sqrt{\frac{q^2}{\lambda}}\epsilon^{*\mu}_\sigma(q)\int d^4x e^{iq\cdot x}\langle V(\tilde{p}, \tilde{\epsilon})|T\{j_{V,\mu}(x), j^\dagger_D(0)\}|0\rangle, \tag{13}$$

where the hadron vector and pseudoscalar current are $j_{V,\mu}(x) = \bar{q}(x)\gamma_\mu c(x)$ and $j^\dagger_D(0) = \bar{c}(0)i\gamma_5 u(0)$, respectively. Here T is the product of the current operator.

In the timelike q^2 region, after inserting the complete intermediate states that have the same quantum numbers $J^P = 0^-$ with the current operator $\bar{c}i\gamma_5 u$ into the hadron current of the correlation function and further isolating the pole term of the lowest pseudoscalar D meson, the correlation function can be read off:

$$\Pi^{\mathrm{H}}_\sigma(p, q) = \sqrt{\frac{q^2}{\lambda}}\left[\frac{\epsilon^{*\mu}_\sigma(q)\langle V|\bar{q}\gamma_\mu c|D\rangle\langle D|\bar{c}i\gamma_5 u|0\rangle}{m^2_D - (p + q)^2} + \sum_{\mathrm{H}}\frac{\epsilon^{*\mu}_\sigma(q)\langle V|\bar{q}\gamma_\mu c|D^{\mathrm{H}}\rangle\langle D^{\mathrm{H}}|\bar{q}i\gamma_5 u|0\rangle}{m^2_{D^{\mathrm{H}}} - (p + q)^2}\right], \tag{14}$$

where $\langle D|\bar{c}i\gamma_5 u|0\rangle = m_D{}^2 f_D/m_c$. After replacing the sum of higher resonances and continuum states with the dispersion integrations, the hadronic representation of the correlator Π^H_σ finally has the form

$$\Pi^{\mathrm{H}}_\sigma(q^2, (p + q)^2) = \frac{m^2_D f_D}{m_c[m^2_D - (p + q)^2]}\mathcal{D}_\sigma(q^2) + \int_{s_0}^\infty \frac{\rho^{\mathrm{H}}_\sigma(s)}{s - (p + q)^2}ds + \text{subtractions.} \tag{15}$$

In the spacelike q^2 region, i.e., $(p+q)^2 - m_c^2 \ll 0$ and $q^2 \ll m_c^2 - O(1 \text{ GeV}^2)$, one needs to contract the c-quark operator by applying a propagator with the gluon field correction:

$$
\langle 0|c_\alpha^i(x)\bar{c}_\beta^j(0)|0\rangle = -i\int \frac{d^4k}{(2\pi)^4} e^{-ik\cdot x}\left\{\delta^{ij}\frac{\not{k}+m_c}{m_c^2-k^2} + g_s\int_0^1 dv\, G^{\mu\nu\alpha}(vx)\left(\frac{\lambda}{2}\right)^{ij}\left[\frac{\not{k}+m_c}{2(m_c^2-k^2)^2}\sigma_{\mu\nu} + \frac{1}{m_c^2-k^2}vx_\mu\gamma_\nu\right]\right\}_{\alpha\beta}.
$$
(16)

For further OPE treatment, one needs the nonlocal matrix elements which are convoluted with the meson light-cone distribution amplitudes (LCDAs) of a growing twist:

$$
\langle V(\tilde{p},\tilde{\epsilon})|\bar{q}_1(x)\sigma_{\mu\nu}q_2(0)|0\rangle = -if_V^\perp\int_0^1 du\, e^{iu(\tilde{p}\cdot x)}\left\{(\tilde{\epsilon}_\mu^*\tilde{p}_\nu - \tilde{\epsilon}_\nu^*\tilde{p}_\mu)\left[\phi_{2;V}^\perp(u) + \frac{m_V^2 x^2}{4}\phi_{4;V}^\perp(u)\right]\right.
$$
$$
+ (\tilde{p}_\mu x_\nu - \tilde{p}_\nu x_\mu)\frac{\tilde{\epsilon}^*\cdot x}{(\tilde{p}\cdot x)^2}m_V^2\left[\phi_{3;V}^\parallel(u) - \frac{1}{2}\phi_{2;V}^\perp(u) - \frac{1}{2}\psi_{4;V}^\perp(u)\right]
$$
$$
\left. + \frac{1}{2}(\tilde{\epsilon}_\mu^* x_\nu - \tilde{\epsilon}_\nu^* x_\mu)\frac{m_V^2}{\tilde{p}\cdot x}[\psi_{4;V}^\perp(u) - \phi_{2;V}^\perp(u)]\right\},
$$
(17)

$$
\langle V(\tilde{p},\tilde{\epsilon})|\bar{q}_1(x)q_2(0)|0\rangle = -\frac{i}{2}f_V^\perp(\tilde{\epsilon}^*\cdot x)m_V^2\int_0^1 du\, e^{iu(\tilde{p}\cdot x)}\psi_{3;V}^\parallel(u),
$$
(18)

$$
\langle V(\tilde{p},\tilde{\epsilon})|\bar{q}_1(x)\gamma_\mu q_2(0)|0\rangle = m_V^2 f_V^\parallel\int_0^1 du\, e^{iu(\tilde{p}\cdot x)}\left\{\frac{\tilde{\epsilon}^*\cdot x}{\tilde{p}\cdot x}\tilde{p}_\mu\left[\phi_{2;V}^\parallel(u) + \frac{m_V^2 x^2}{4}\phi_{4;V}^\parallel(u)\right]\right.
$$
$$
\left. + \left(\tilde{\epsilon}_\mu^* - \tilde{p}_\mu\frac{\tilde{\epsilon}^*\cdot x}{p\cdot x}\right)\phi_{3;V}^\perp(u) - \frac{1}{2}m_V^2 x_\mu\frac{\tilde{\epsilon}^*\cdot x}{(\tilde{p}\cdot x)^2}[\psi_{4;V}^\parallel(u) + \phi_{2;V}^\parallel(u) - 2\phi_{3;V}^\perp(u)]\right\},
$$
(19)

$$
\langle V(\tilde{p},\tilde{\epsilon})|\bar{q}_1(x)\gamma_\mu\gamma_5 q_2(0)|0\rangle = -\frac{1}{4}m_V f_V^\parallel \varepsilon^{\mu\nu\alpha\beta}\tilde{\epsilon}_\mu^*\tilde{p}_\alpha x_\beta\int_0^1 du\, e^{iu(\tilde{p}\cdot x)}\psi_{3;V}^\perp(u),
$$
(20)

where $V = \rho, \omega, K^*$ mesons and $q_1 = d(s)$ for the ρ, ω, K^* mesons.

After replacing those hadronic matric elements and subtracting the contribution of the continuum spectrum using dispersion integration, one can finish the QCD representation calculation. In this paper, we will not consider the three-particle part due to its negligible contribution. Specifically, it is no more than 0.3% of the total TFFs, and a more detailed analysis can be obtained from our previous study [60].

Moreover, one needs to equate the two types of representations of the correlator and subtract the contributions from higher resonances and continuum states. With the help of the Borel transformation, the LCSR for $D \to V$ HFFs can finally be read off:

$$
\mathcal{D}_{V,0}(q^2) = \int_0^1 du\, e^{(m_D^2-s)/M^2}\frac{m_c f_V^\perp \mathcal{F}}{2\sqrt{\lambda}m_V m_D^2 f_D}\left\{2\mathcal{S}\Theta(c(u,s_0))\phi_{2;V}^\perp(u)\right.
$$
$$
- \frac{\lambda m_c m_V \tilde{f}_V}{u^2 M^2}\widetilde{\Theta}(c(u,s_0))\Phi_{2;V}^\parallel(u) - (\tilde{m}_q m_V \tilde{f}_V - m_V^2)\left[\mathcal{F}\Theta(c(u,s_0)) - \lambda\frac{1}{uM^2}\widetilde{\Theta}(c(u,s_0))\right]\psi_{3;V}^\parallel(u)
$$
$$
+ m_c m_V \tilde{f}_V\left[\frac{\lambda}{u^2 M^2}\widetilde{\Theta}(c(u,s_0))\Phi_{3;V}^\perp(u) + \mathcal{F}\Theta(c(u,s_0))\phi_{3;V}^\perp(u)\right] + m_V^2 \mathcal{S}\left[\frac{\mathcal{N}}{2u^3 M^4}\widetilde{\widetilde{\Theta}}(c(u,s_0))\right.
$$
$$
\left. - \frac{3}{2u^2 M^2}\widetilde{\Theta}(c(u,s_0))\right]\phi_{4;V}^\perp(u) - \left[\frac{\lambda\mathcal{S}}{2u^3 M^4}\widetilde{\widetilde{\Theta}}(c(u,s_0)) - m_V^2\frac{\mathcal{S}-4\lambda}{u^2 M^2}\right]\widetilde{\Theta}(c(u,s_0))I_L(u)
$$
$$
- \frac{\lambda m_c^3 m_V^3 \tilde{f}_V}{u^4 M^6}\widetilde{\widetilde{\Theta}}(c(u,s_0))\Phi_{4;V}^\perp(u) + m_c m_V^3 \tilde{f}_V\left[\frac{\lambda}{u^2 M^4}\widetilde{\widetilde{\Theta}}(c(u,s_0)) + \frac{\mathcal{F}}{u^2 M^2}\widetilde{\Theta}(c(u,s_0))\right]C_V(u)
$$
$$
\left. - m_V^2\left[\frac{3}{2}\Theta(c(u,s_0)) + \left(\frac{\mathcal{N}}{u^2 M^2} - \frac{\lambda}{2uM^2\mathcal{F}}\right)\widetilde{\Theta}(c(u,s_0))\right]H_3(u)\right\},
$$
(21)

$$
\mathcal{D}_{V,1}(q^2) = \int_0^1 du\, e^{(m_D^2-s)/M^2}\frac{m_c f_V^\perp\sqrt{2q^2}}{2m_D^2 f_D}\left\{\Theta(c(u,s_0))\phi_{2;V}^\perp(u) + m_V^2\left[\frac{\mathcal{N}}{u^3 M^4}\widetilde{\widetilde{\Theta}}(c(u,s_0))\right.\right.
$$
$$
\left.\left. + \frac{3}{u^2 M^2}\widetilde{\Theta}(c(u,s_0))\right]\phi_{4;V}^\perp(u) - \frac{m_V m_c \tilde{f}_V}{2u^2 M^2}\widetilde{\Theta}(c(u,s_0))\psi_{3;V}^\perp(u)\right\},
$$
(22)

$$\mathcal{D}_{V,2}(q^2) = \int_0^1 du e^{(m_D^2 - s)/M^2} \frac{\sqrt{2q^2} m_c f_V^\perp}{2\sqrt{\lambda} m_D^2 f_D} \left\{ \mathcal{E}\,\Theta(c(u,s_0))\phi_{2;V}^\perp(u) - 2\,\Theta(c(u,s_0))\left(\tilde{f}_V m_V \tilde{m}_q - m_V^2\right)\psi_{3;V}^\parallel(u) \right.$$

$$+ m_V^2 \mathcal{E}\left[\frac{\mathcal{N}}{u^3 M^4}\widetilde{\widetilde{\Theta}}(c(u,s_0)) + \frac{3}{u^2 M^2}\widetilde{\Theta}(c(u,s_0))\right]\phi_{4;V}^\perp(u) + \frac{2m_V^2}{u^2 M^2}\mathcal{E}\widetilde{\Theta}(c(u,s_0))I_L(u)$$

$$- m_V^2\left[3\Theta(c(u,s_0)) + \frac{2\mathcal{N}}{u^2 M^2}\widetilde{\Theta}(c(u,s_0))\right]H_3(u) - 2m_c \tilde{f}_V m_V \Theta(c(u,s_0))\phi_{3;V}^\perp(u)$$

$$\left. - \frac{2m_c m_V^3 \tilde{f}_V}{u^2 M^2}\widetilde{\Theta}(c(u,s_0))C_V(u)\right\}, \tag{23}$$

$$\mathcal{D}_{V,t}(q^2) = \int_0^1 du\, e^{(m_D^2 - s)/M^2} \frac{m_c m_V f_V^\perp}{2m_V m_D^2 f_D}\left\{ um_V \Theta(c(u,s_0))\phi_{2;V}^\perp(u) - \frac{m_c \tilde{f}_V \mathcal{F}}{u^2 M^2}\widetilde{\Theta}(c(u,s_0))\Phi_{2;V}^\parallel(u) \right.$$

$$- (\tilde{m}_q \tilde{f}_V - m_V)\left[\Theta(c(u,s_0)) + \frac{u\mathcal{F} + 2q^2}{u^2 M^2}\widetilde{\Theta}(c(u,s_0))\right]\psi_{3;V}^\parallel(u) - m_c \tilde{f}_V \Theta(c(u,s_0))\phi_{3;V}^\perp(u)$$

$$+ m_c \tilde{f}_V \frac{\mathcal{F}}{u^2 M^2}\widetilde{\Theta}(c(u,s_0))\Phi_{3;V}^\perp(u) + m_V^3\left[\frac{\mathcal{N}}{u^2 M^4}\widetilde{\widetilde{\Theta}}(c(u,s_0)) + \frac{3}{uM^2}\widetilde{\Theta}(c(u,s_0))\right]\phi_{4;V}^\perp(u)$$

$$+ m_c^3 m_V^2 \tilde{f}_V \frac{\mathcal{F}}{u^4 M^6}\widetilde{\widetilde{\Theta}}(c(u,s_0))\Phi_{4;V}^\parallel(u) - m_V\left[\frac{\mathcal{E}}{2uM^2}\widetilde{\Theta}(c(u,s_0)) + \frac{3}{2}\Theta(c(u,s_0))\right]H_3(u)$$

$$- m_V\left[\frac{9\mathcal{F} - 2um_V^2 + 15q^2}{u^2 M^2}\widetilde{\Theta}(c(u,s_0)) + \frac{\mathcal{W}}{u^3 M^4}\widetilde{\widetilde{\Theta}}(c(u,s_0))\right]I_L(u)$$

$$\left. + \frac{m_c \tilde{f}_V}{2}\left[\frac{2m_V^2}{u^2 M^2}\widetilde{\Theta}(c(u,s_0)) + \frac{\mathcal{S}}{u^3 M^4}\widetilde{\widetilde{\Theta}}(c(u,s_0))\right]C_V(u)\right\}, \tag{24}$$

where $\mathcal{E} = m_D^2 + \xi m_V^2 - q^2$, $\mathcal{F} = m_D^2 - m_V^2 - q^2$, $\mathcal{N} = um_D^2 - u\bar{u}m_V^2 + \bar{u}q^2$, $\mathcal{S} = 2m_V^2[um_D^2 - um_V^2 + (1-\bar{u})q^2]$, $\mathcal{W} = 2m_D^2[-u\xi m_V^2 + q^2(1 + u + u\bar{u})] + u\xi(m_D^4 + m_V^4) - 2q^2(1+u)\bar{u}m_V^2 - q^4(2+u)$, and $s = [m_b^2 - \bar{u}(q^2 - um_V^2)]/u$, with $\bar{u} = 1 - u$, $\xi = 2u - 1$. The effective decay constant $\tilde{f}_V = f_V^\parallel/f_V^\perp$, and simplified distribution functions $\Phi_{2;V}^\parallel(u)$, $\Phi_{3;V}^\perp(u)$, $\Phi_{4;V}^\perp(u)$, $I_L(u)$, and $H_3(u)$ are defined as

$$\Phi_{2;V}^\parallel(u) = \int_0^u dv\phi_{2;V}^\parallel(u), \quad \Phi_{3;V}^\perp(u) = \int_0^u dv\phi_{3;V}^\perp(u), \quad \Phi_{4;V}^\perp(u) = \int_0^u dv\phi_{4;V}^\perp(u), \quad H_3(u) = \int_0^u dv[\psi_{4;V}^\perp(v) - \phi_{2;V}^\perp(v)],$$

$$I_L(u) = \int_0^u dv \int_0^v dw\left[\phi_{3;V}^\parallel(w) - \frac{1}{2}\phi_{2;V}^\perp(w) - \frac{1}{2}\psi_{4;V}^\perp(w)\right], \quad C_V(u) = \int_0^u dv \int_0^v dw[\psi_{4;V}^\parallel(w) + \phi_{2;V}^\parallel(w) - 2\phi_{3;V}^\perp(w)]. \tag{25}$$

$\Theta(c(u,s_0))$ is the conventional step function, and $\widetilde{\Theta}[c(u,s_0)]$ and $\widetilde{\widetilde{\Theta}}(c(u,s_0))$ are defined as

$$\int_0^1 \frac{du}{u^2 M^2}e^{-s/M^2}\widetilde{\Theta}(c(u,s_0))f(u) = \int_{u_0}^1 \frac{du}{u^2 M^2}e^{-s)/M^2}f(u) + \delta(c(u_0,s_0)), \tag{26}$$

$$\int_0^1 \frac{du}{2u^3 M^4}e^{-s/M^2}\widetilde{\widetilde{\Theta}}(c(u,s_0))f(u) = \int_{u_0}^1 \frac{du}{2u^3 M^4}e^{-s/M^2}f(u) + \Delta(c(u_0,s_0)), \tag{27}$$

where

$$\delta(c(u,s_0)) = e^{-s_0/M^2}\frac{f(u_0)}{\mathcal{C}_0}, \quad \Delta(c(u,s_0)) = e^{-s_0/M^2}\left[\frac{1}{2u_0 M^2}\frac{f(u_0)}{\mathcal{C}_0} - \frac{u_0^2}{2\mathcal{C}_0}\frac{d}{du}\left(\frac{f(u)}{u\mathcal{C}}\right)\Big|_{u=u_0}\right],$$

$\mathcal{C}_0 = m_b^2 + u_0^2 m_V^2 - q^2$, and u_0 is the solution of $c(u_0, s_0) = 0$, with $0 \leqslant u_0 \leqslant 1$. Numerically, we observe that the leading-twist terms are dominant for the LCSRs of the HFFs, which agrees well with the usual δ-power counting rule. Thus, those HFFs will provide us with a useful platform for testing the properties of the leading-twist LCDAs via comparisons with the data or predictions in other theoretical approaches.

III. NUMERICAL ANALYSIS

For the numerical analysis, the input parameters are taken as follows. The masses of mesons are $m_D = 1.865$ GeV, $m_\rho = 0.775$ GeV, $m_\omega = 0.782$ GeV, and $m_{K^*} = 0.892$ GeV. The c-quark pole mass $m_c = 1.28(3)$ GeV is taken from

the particle data group [58]. For the decay constants, we take $f_D = 0.204(5)$ for the D meson, $f_\rho^\parallel = 0.198(7)$ and $f_\rho^\perp = 0.160(10)$ for the ρ meson, $f_\omega^\parallel = 0.195(3)$ and $f_\omega^\perp = 0.145(10)$ for the ω meson, and $f_{K^*}^\parallel = 0.226(28)$ and $f_{K^*}^\perp = 0.185(10)$ for the K^* meson [50]. The Cabibbo-Kobayashi-

Maskawa matrix elements are $|V_{cd}| = 0.216$ and $|V_{cs}| = 0.997$.

A. LCDAs and $D \to V$ HFFs

Within the QCD LCSR framework, HFFs will be expressed by different twist LCDAs due to the same method for handling the correlation function to get the TFFs. The resultant HFFs contain twist-2, -3, -4 LCDAs. Next, we will discuss the associated LCDAs and parameters.

For the leading twist LCDAs, their conformal expansion can be expressed in terms of Gegenbauer polynomials,

$$\phi_{2;V}^{\|,\perp}(u, \mu^2) = \phi_{\rm asy}(u)\left[1 + \sum a_n(\mu^2)C_n^{3/2}(\xi)\right]. \quad (28)$$

Here $\phi_{\rm asy}(u) = 6u\bar{u}$ stands for the asymptotic DA. $\phi_{2;V}^{\|,\perp}(u, \mu^2)$ will equal to $\phi_{\rm asy}(u)$ in the limit $\mu^2 \to \infty$. To make a comparison with other theoretical and experimental predictions, the twist-2, -3, -4 LCDAs' moments and coupling constants are referred to Ball [61] and are calculated within the Shifman-Vainshtein-Zakharov (SVZ) QCD sum rule taken by many theoretical groups. The analytical expression and values are listed in the Appendix.

Then, there are two internal parameters, i.e., continuum threshold s_0 and Borel windows M^2. The former is a demarcation for the D-meson ground state and higher mass contributions. Specifically, we take the continuum thresholds s_0 for $D \to V$ HFFs $\mathcal{D}_{V,0}(q^2)$, $\mathcal{D}_{V,1}(q^2)$, $\mathcal{D}_{V,2}(q^2)$, and $\mathcal{D}_{V,t}(q^2)$ as $s_{\rho,0} = 4.0(3)$, $s_{\rho,1} = 4.0(3)$, $s_{\rho,2} = 4.0(3)$, $s_{\rho,t} = 4.5(3)$, $s_{\omega,0} = 3.6(3)$, $s_{\omega,1} = 6.5(3)$, $s_{\omega,2} = 4.0(3)$, $s_{\omega,t} = 4.0(3)$, $s_{K^*,0} = 4.0(3)$, $s_{K^*,1} = 6.0(3)$, $s_{K^*,2} = 4.0(3)$, and $s_{K^*,t} = 3.7(3)$.

To determine the Borel parameters for the $D \to V$ HFFs, we adopt the following three criteria:

(i) We require the continuum contribution to be less than 35% of the total LCSR.

(ii) We require all the high-twist LCDA contributions to be less than 15% of the total LCSR.

(iii) The derivatives of LCSRs for HFFs with respect to $(-1/M^2)$ give four LCSRs for the D-meson mass m_D. We require the predicted D-meson mass to be fulfilled compared with the experiment one, i.e., $|m_D^{\rm th} - m_D^{\rm exp}|/m_D^{\rm exp} \leqslant 0.1\%$.

Thus, the obtained Borel windows $M^2({\rm GeV}^2)$ are $M_{\rho,0}^2 = 2.5(3)$, $M_{\rho,1}^2 = 4.0(3)$, $M_{\rho,2}^2 = 3.5(3)$, $M_{\rho,t}^2 = 3.0(3)$, $M_{\omega,0}^2 = 2.5(3)$, $M_{\omega,1}^2 = 4.8(3)$, $M_{\omega,2}^2 = 3.0(3)$, $M_{\omega,t}^2 = 3.0(3)$, $M_{K^*,0}^2 = 2.5(3)$, $M_{K^*,1}^2 = 6.0(3)$, $M_{K^*,2}^2 = 4.0(3)$, and $M_{K^*,t}^2 = 2.7(3)$.

The reliable regions for the D-meson semileptonic decays within the LCSR approach can be set at $0 \leqslant q^2 \leqslant q_{\rm LCSR,max}^2 \approx 0.8\,{\rm GeV}^2$. Meanwhile, the allowable physical range of the momentum transfer is $0 \leqslant q^2 \leqslant q_{V,\rm max}^2$, with

$$q_{\rho,\rm max}^2 = (m_D - m_\rho)^2 \simeq 1.18\,{\rm GeV}^2,$$
$$q_{\omega,\rm max}^2 = (m_D - m_\omega)^2 \simeq 1.17\,{\rm GeV}^2,$$
$$q_{K^*,\rm max}^2 = (m_D - m_{K^*})^2 \simeq 0.98\,{\rm GeV}^2$$

for ρ, ω, and K^* mesons, respectively. Then, we use the SSE to do the extrapolation for the HFFs based on the analyticity

TABLE II. The fitted parameters $a_{0;1;2}^V$ for the HFFs $\mathcal{D}_{V,\sigma}$, where all input parameters are set to their central values.

	$\mathcal{D}_{V,0}$	$\mathcal{D}_{V,1}$	$\mathcal{D}_{V,2}$	$\mathcal{D}_{V,t}$
a_0^ρ	1.841	1.187	4.257	0.913
a_1^ρ	-68.95	-5.177	-137.2	-18.49
a_2^ρ	-879.8	-88.14	1774	160.2
Δ_ρ	0.000	0.008	0.042	0.000
a_0^ω	1.786	0.763	4.666	0.868
a_1^ω	-68.41	-1.125	-162.6	-18.46
a_2^ω	883.8	-22.53	2163	170.1
Δ_ω	0.000	0.001	0.050	0.000
$a_0^{K^*}$	1.937	0.941	5.074	0.975
$a_1^{K^*}$	-91.04	2.976	-209.4	-21.97
$a_2^{K^*}$	1438	-70.30	3545	181.0
Δ_{K^*}	0.000	0.001	0.031	0.000

and unitarity consideration. The extrapolation of the HFFs satisfies the following parameterized formulas:

$$\mathcal{D}_{V,0}(t) = \frac{1}{B(t)\sqrt{z(t,t_-)}\phi_T^{V-A}(t)} \sum_{k=0,1,2} a_k^{V,0} z^k, \quad (29)$$

$$\mathcal{D}_{V,1}(t) = \frac{\sqrt{-z(t,0)}}{B(t)\phi_T^{V-A}(t)} \sum_{k=0,1,2} a_k^{V,1} z^k, \quad (30)$$

$$\mathcal{D}_{V,2}(t) = \frac{\sqrt{-z(t,0)}}{B(t)\sqrt{z(t,t_-)}\phi_T^{V-A}(t)} \sum_{k=0,1,2} a_k^{V,2} z^k, \quad (31)$$

$$\mathcal{D}_{V,t}(t) = \frac{1}{B(t)\phi_L^{V-A}(t)} \sum_{k=0,1,2} a_k^{V,t} z^k, \quad (32)$$

where $\phi_I^X(t) = 1$, $\sqrt{-z(t,0)} = \sqrt{q^2}/m_D$, $B(t) = 1 - q^2/m_\sigma^2$, $\sqrt{z(t,t_-)} = \sqrt{\lambda}/m_D^2$, and

$$z(t) = \frac{\sqrt{t_+ - t} - \sqrt{t_+ - t_0}}{\sqrt{t_+ - t} + \sqrt{t_+ - t_0}},$$

with $t_\pm = (m_D \pm m_V)^2$ and $t_0 = t_+(1 - \sqrt{1 - t_-/t_+})$.

The parameters a_k^σ can be determined by requiring the "quality" of fit Δ_V to be less than 1, which is defined as

$$\Delta_V = \frac{\sum_t \left|\mathcal{D}_{V,\sigma}(t) - \mathcal{D}_{V,\sigma}^{\rm fit}(t)\right|}{\sum_t \left|\mathcal{D}_{V,\sigma}(t)\right|} \times 100, \quad (33)$$

where $t \in [0, 0.02, \ldots, 0.58, 0.8]\,{\rm GeV}^2$. We put the determined parameters $a_k^{V,\sigma}$ in Table II, in which all the input parameters are set to their central values.

The extrapolated HFFs in the whole q^2 region are presented in Fig. 2, where the shaded bands are uncertainties from various input parameters. The shapes of the HFFs for the three vector mesons are similar due to the same analytic expression and little-varied input parameters. We can see $\mathcal{D}_{V,(1;2)} = 0$ at $q^2 = 0\,{\rm GeV}^2$, which is caused by the coefficient q^2 of $\mathcal{D}_{V,(1;2)}(q^2)$. The q^2 coefficient also depresses the error of HFFs $\mathcal{D}_{V,(1;2)}(q^2)$ for the smaller q^2, which can be directly seen from Fig. 2. Meanwhile, this depressed effect can be directly transmitted to the differential transversal decay width in Fig. 3, as seen in the next section.
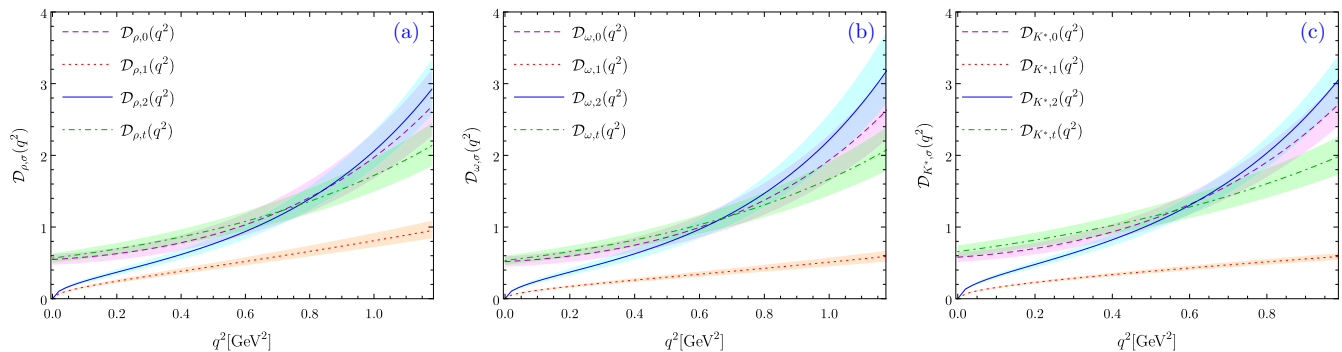
FIG. 2. The extrapolated LCSR prediction HFFs $\mathcal{D}_{V,\sigma}(q^2)$ for $D \to V$ with $V = \rho, \omega, K^*$ mesons. The solid lines represent the center values, and the shaded bands corresponds to their uncertainties. The maximum extrapolated physically allowable points q^2 are $q^2_{\rho,\max} = (m_D - m_\rho)^2 \simeq 1.18 \, \mathrm{GeV}^2$, $q^2_{\omega,\max} = (m_D - m_\omega)^2 \simeq 1.17 \, \mathrm{GeV}^2$, and $q^2_{K^*,\max} = (m_D - m^*_K)^2 \simeq 0.98 \, \mathrm{GeV}^2$ for ρ, ω, and K^* mesons, respectively.

B. *D*-meson semileptonic decays

The HFFs extracted from the LCSRs are employed to study the *D*-meson semileptonic decay, i.e., the decay width, branching fractions, longitudinal and transverse polarizations, forward-backward asymmetry, and lepton-side convexity parameter, which are frequently used for the precision test of the SM and the search for new physics beyond SM.

1. Decay width

In this part, we probe the decay width of $D \to V$ semilepton decay by applying Eqs. (4), (6), and (7). First, we present the LCSR predictions for the polarization differential decay widths $1/|V_{cq}|^2 \times d\Gamma^L/dq^2$ and $1/|V_{cq}|^2 \times d\Gamma^T/dq^2$ and the total differential decay widths $1/|V_{cq}|^2 \times d\Gamma/dq^2$ in Fig. 3, in which the dashed, dotted, and solid lines represent the corresponding central values; the uncertainties are a result of the square average of all input parameters.

For the central lines of the differential decay width in Fig. 3, we find that there is a similar behavior for all of the differential decay widths with $|V_{cq}|$ independent of $D \to V \ell^+ \nu_\ell$ semileptonic decays. Both the total differential width and transversal differential width increase first and then decrease with q^2. The longitudinal differential width is almost unchanged from the small- to intermediate-q^2 region, while it drops sharply in the large q^2 region. In addition, the longitudinal differential width dominates the small-q^2 region, while the transversal differential width dominates the large-q^2 region. The position of the alternating point of the dominant q^2 region is near the midpoint of the whole physical feasible region, which is represented by the red stars in Fig. 3, i.e., $q^2_{\min,(\rho,\omega,K^*)} = (0.51, 0.54, 0.49) \, \mathrm{GeV}^2$.

The three figures (Fig. 3) imply that the total width decreases as the final meson mass increases, which is intuitive from Table III. There are three main reasons to justify this:

(i) The physical feasible regions q^2 decrease from the left to right in Fig. 3, which is caused by the increasing mass of the final meson.

(ii) The peak of the longitudinal and transversal differential width decreases from the left to right panel in Fig. 3.

(iii) The trend of the curves for longitudinal and transverse differential widths is almost the same for the three channels in Fig. 3.

For comparison, the central values of the total differential width of BESIII [16,23,24] are also shown in Fig. 3. We observe that the curves of BESIII are in agreement with our predictions, within the error bars. But there is a significantly different shape for the center curves, especially for the large-q^2 region. The main reason is that BESIII uses the unipolar point continuation extrapolation method, while HFFs need to use the SSE extrapolation method.

Then we show the total decay widths $\Gamma/|V_{cq}|^2$, $\Gamma^L/|V_{cq}|^2$, and $\Gamma^T/|V_{cq}|^2$ in Table III. The three kinds of total decay widths decrease as the final meson mass increases, which is consistent with Fig. 3. There is also an interesting phenomenon: it is almost identical for both total decay width $\Gamma^L/|V_{cq}|^2$ and $\Gamma^T/|V_{cq}|^2$ gaps between different decay channels. We list the ratio Γ^L/Γ^T for the $D \to V \ell^+ \nu_\ell$ semileptonic decays in Table IV. As a comparison, we also present other theoretical predictions, i.e., heavy meson and chiral Lagrangians (HMχT) [51], the covariant confining quark model (CCQM) [59], the covariant quark model (CQM) [62], LCSR [63], the QCD sum rule (QCDSR) [64], and the lattice QCD (LQCD) [65]. All of our predictions for the ratio Γ^L/Γ^T agree with that of the CCQM within the error bars. Although the rest of the theoretical predictions are incomplete for the ratio Γ^L/Γ^T, again, our results are in good agreement with them within the error bars, except for QCDSR results.

As a further step, we calculate the branching fractions of $D \to V \ell^+ \nu_\ell$ by employing $\tau(D^0) = 0.410(2) \, \mathrm{ps}$ and $\tau(D^+) = 1.040(7) \, \mathrm{ps}$; the results are collected in Table V. Compared with other theoretical and LQCD [65] predictions, our results are small, which is more consistent with the BESIII [16,23,24] experiment within the error bars. The reasons are that we adopt HFFs to deal with the $D \to V$ hadronic matrix elements, where HFFs are calculated using the QCD LCSR approach and the corresponding physical observations

TABLE III. The total decay widths $\Gamma/|V_{cq}|^2$, $\Gamma^L/|V_{cq}|^2$, and $\Gamma^T/|V_{cq}|^2$ (in units of 10^{-15} GeV) for the central values.

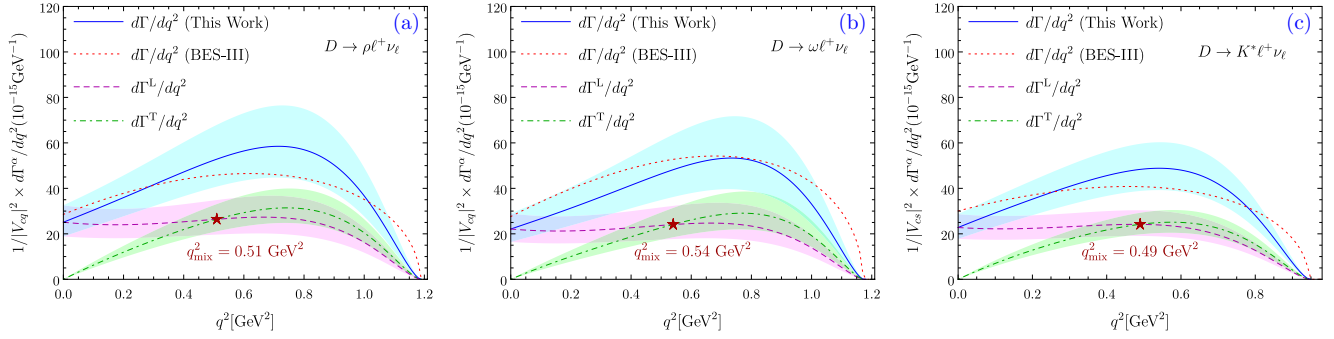|	$\Gamma/|V_{cq}|^2$	$\Gamma^L/|V_{cq}|^2$	$\Gamma^T/|V_{cq}|^2$
$D \to \rho \ell^+ \nu_\ell$	49.564	26.299	23.265
$D \to \omega \ell^+ \nu_\ell$	44.108	23.320	20.788
$D \to K^* \ell^+ \nu_\ell$	33.631	18.539	15.092

FIG. 3. The LCSR predictions for the polarized differential decay widths $1/|V_{cq}|^2 \times d\Gamma^{L,T}/dq^2$ and the total differential decay widths $1/|V_{cq}|^2 \times d\Gamma/dq^2$ for ρ, ω, K^* mesons, in which the dashed, dash-dotted, and solid lines represent the corresponding central values and the shaded bands are the squared average of all the input parameters. For comparison, we also present the BESIII predictions [16,23,24].

are further investigated. Compared with the traditional TFF parameterized method for the hadronic matrix elements, the HFF parameterized method has some advantages:

(i) As mentioned in the Introduction of our paper, the HFFs parameterized method facilitates the study of tracking polarization.

(ii) According to the diagonalizable unitarity relations, one can get the dispersive bound for the HFF parametrization.

In addition, there are many theoretical approaches for dealing with the form factors for the $D \to V$ decays processes, such as LCSR used in this paper, the LQCD, the perturbative QCD (pQCD), and so on. The pQCD, LCSR, and LQCD approaches are valid in the small-q^2 region, in the small- and intermediate-q^2 region, and in the large-q^2 region, respectively. The LCSR approach has the advantage that it can be extrapolated to the whole q^2 region and provides an important bridge for connecting various approaches.

2. Polarization observations

Due to the current experimental conditions, it is difficult to measure the q^2 dependence of the polarization observation. However, it is very important to study the q^2 dependence on these observables. On the one hand, it can facilitate the comparison among different theories; on the other hand, it also provides references for experimental research on q^2 dependence and more details for exploring new physics.

We first show the final state polarizations $P^\ell_{L,T}$ and $F^\ell_{L,T}$ in Fig. 4.

(i) For the top parts, the final lepton polarization for $D \to V(\rho, \omega, K^*)\ell^+\nu_\ell$ is shown and calculated by applying Eq. (8). All lepton polarizations $P^\ell_{L,T}$ exhibit similar behavior. In the

large-q^2 region, all $P_{L,T}$ are almost unchanged, except that P^μ_T rises slowly with the increase of q^2, i.e., $P^\ell_L \approx 1$, $P^e_T \approx 0$, and $P^e_T \lesssim 0$. In the small-q^2 region, all $P_{L,T}$ polarities are singular due to the δ_ℓ factor, which is clearly shown in the corresponding inset with the logarithmic axis. We observe that $P^{e(\mu)}_L$ are approximately equal to -0.4 at $q^2_{\min} = m^2_{e(\mu)}$. As q^2 increases, $P^{e(\mu)}_L$ then rapidly increases to close to 1 and finally remains stable. For the transverse component, $P^{e,\mu}_T(q^2_{\min} = m^2_{e(\mu)}) \approx -0.8$. As q^2 increases, P^μ_T rapidly increases to close to zero and then remains stable, while P^e_T increase rapidly and then moderately.

(ii) For the bottom parts, the longitudinal $F^\ell_L(q^2)$ and transverse $F^\ell_T(q^2)$ polarization fractions of the vector meson are shown and calculated by using Eq. (8), which indicates the three kinds of vector ρ, ω, K^* mesons have a similar behavior for both $F^\ell_L(q^2)$ and $F^\ell_T(q^2)$. In all the allowed physical regions, we have $F^\ell_L(q^2) + F^\ell_T(q^2) = 1$. For the large recoil point $q^2 = 0\,\text{GeV}^2$, we observe $F^\ell_L(0) = 1$ and $F^\ell_T(0) = 0$. As q^2 increases, $F^\ell_L(q^2)$ monotonically decreases, and $F^\ell_T(q^2)$ reverses. In addition, $F^\ell_L(q^2)$ is dominant in the small-q^2 regions, while $F_T(q^2)$ is dominant in the large-q^2 regions. The position of the alternating point of the dominant q^2 region is near the midpoint of the whole physically feasible region. At the alternating point q^2_{mix}, we observe $F^\ell_L = F^\ell_T = 0.5$ according to the relation $F^\ell_L(q^2) + F^\ell_T(q^2) = 1$.

We then plot the forward-backward asymmetry $\mathcal{A}^\ell_{FB}$ and the lepton-side $\mathcal{C}^\ell_F(q^2)$ convexity parameter in Fig. 5.

(i) The top parts of Fig. 5 show the change in forward-backward asymmetry $\mathcal{A}^\ell_{FB}$ from $q^2_{\min} = m^2_\ell$ to $q^2_{\max} = (m_D - m_V)^2$. All $\mathcal{A}^\ell_{FB}$ first decrease from a positive value to zero

TABLE IV. Ratio Γ^L/Γ^T for the $D \to V(\rho, \omega, K^*)\ell^+\nu_\ell$ semileptonic decays, where the uncertainties are the square average of all the input parameters. The theoretical and lattice results are listed for comparison. Note that the lepton mass is ignored in $HM\chi T$ [51]. For convenience, we list it in the $D \to Xe^+\nu_e$ case because the electron mass is too small to ignore.

	This work	HMχT [51]	CCQM [59]	CQM [62]	LCSR [63]	QCDSR [64]	LQCD [65]
$D \to \rho e^+\nu_e$	$1.130^{+0.095}_{-0.133}$	1.10	1.13	1.16	1.17(9)	0.86(6)	
$D \to \rho\mu^+\nu_\mu$	$1.119^{+0.095}_{-0.132}$		1.04				
$D \to \omega e^+\nu_e$	$1.122^{+0.042}_{-0.075}$	1.10	1.10				
$D \to \omega\mu^+\nu_\mu$	$1.110^{+0.042}_{-0.074}$		1.02				
$D \to K^* e^+\nu_e$	$1.228^{+0.061}_{-0.074}$	1.13	1.18	1.28	1.15(10)		1.2(3)
$D \to K^*\mu^+\nu_\mu$	$1.212^{+0.060}_{-0.073}$		1.07				

TABLE V. Branching fractions for semileptonic D decays, i.e., $D \to V(\rho, \omega, K^*)\ell^+\nu_\ell$ (values are times 10^{-3} for ρ and ω mesons and times 10^{-2} for K^* mesons), where the uncertainties are the square averages of all the input parameters. The current theoretical and experimental results in the literature are also listed as a comparison. Note that the lepton mass is ignored in HMχT. [51]. For convenience, we list it in the $D \to Xe^+\nu_e$ case because the electron mass is too small to ignore.

	$D^0 \to \rho^- e^+ \nu_e$	$D^0 \to \rho^- \mu^+ \nu_\mu$	$D^+ \to \rho^0 e^+ \nu_e$	$D^+ \to \rho^0 \mu^+ \nu_\mu$	$D^+ \to \omega e^+ \nu_e$
This work	$1.440^{+0.277}_{-0.250}$	$1.432^{+0.274}_{-0.248}$	$1.827^{+0.351}_{-0.317}$	$1.816^{+0.348}_{-0.314}$	$1.740^{+0.482}_{-0.399}$
HMχT [51]	2.0		2.5		2.5
CCQM [59]	1.62	1.55	2.09	2.01	1.85
LFQM [66]					2.1(2)
χUA [67]	1.97	1.84	2.54	2.37	2.46
LCSR [68]	$1.81^{+0.18}_{-0.13}$	$1.73^{+0.17}_{-0.13}$	$2.29^{+0.23}_{-0.16}$	$2.20^{+0.21}_{-0.16}$	$1.93^{+0.20}_{-0.14}$
LQCD [65]			2.23(70)	2.13(64)	
BESIII [16,23,24]	1.445(70)		1.860(93)		1.63(14)
CLEO [20–22]	1.77(16)		$2.17(12)(^{+0.12}_{-0.22})$		1.82(19)
PDG [58]				2.4(4)	

	$D^+ \to \omega \mu^+ \nu_\mu$	$D^0 \to K^{*-} e^+ \nu_e$	$D^0 \to K^{*-} \mu^+ \nu_\mu$	$D^+ \to \bar{K}^{*0} e^+ \nu_e$	$D^+ \to \bar{K}^{*0} \mu^+ \nu_\mu$
This work	$1.728^{+0.479}_{-0.397}$	$2.082^{+0.334}_{-0.314}$	$2.066^{+0.330}_{-0.310}$	$5.282^{+0.847}_{-0.796}$	$5.242^{+0.838}_{-0.787}$
HMχT [51]		2.2		5.6	
CCQM [59]	1.78	2.96	2.80	7.61	7.21
LFQM [66]	2.0(2)			7.5(7)	7.0(7)
χUA [67]	2.29	2.15	1.98	5.56	5.12
LCSR [68]	$1.85^{+0.19}_{-0.13}$	2.12(9)	$2.01^{+0.09}_{-0.08}$	$5.37^{+0.24}_{-0.23}$	$5.10^{+0.23}_{-0.21}$
LQCD [65]				6.26(184)	5.95(167)
BESIII [16,23,24]	1.77(29)	2.033(66)			
CLEO [20–22]		2.16(17)			5.27 ± 0.16
PDG [58]				5.4(1)	
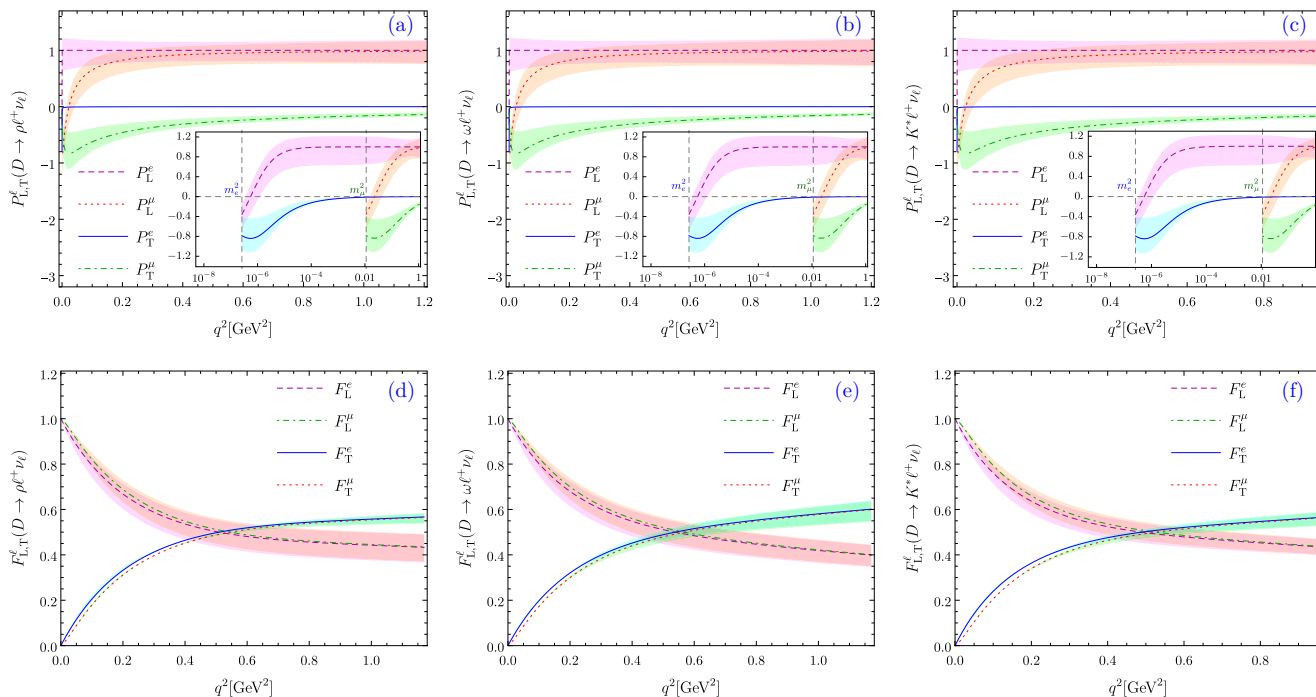
FIG. 4. The final state polarization $P^\ell_{\text{L,T}}$ and $F^\ell_{\text{L,T}}$ as a function of q^2 for $D \to V\ell^+\nu_\ell$. Here P and F represent a charged lepton and vector meson in the final state, which correspond to the upper and bottom parts, respectively. The symbols T and L stand for longitudinal and transverse fractions; V stands for the ρ, ω, K^* mesons, corresponding to the left, medial, and right parts, respectively. The dashed, dotted, dot-dashed, and solid lines represent the corresponding central values, and the shaded bands are the corresponding errors from HFFs.
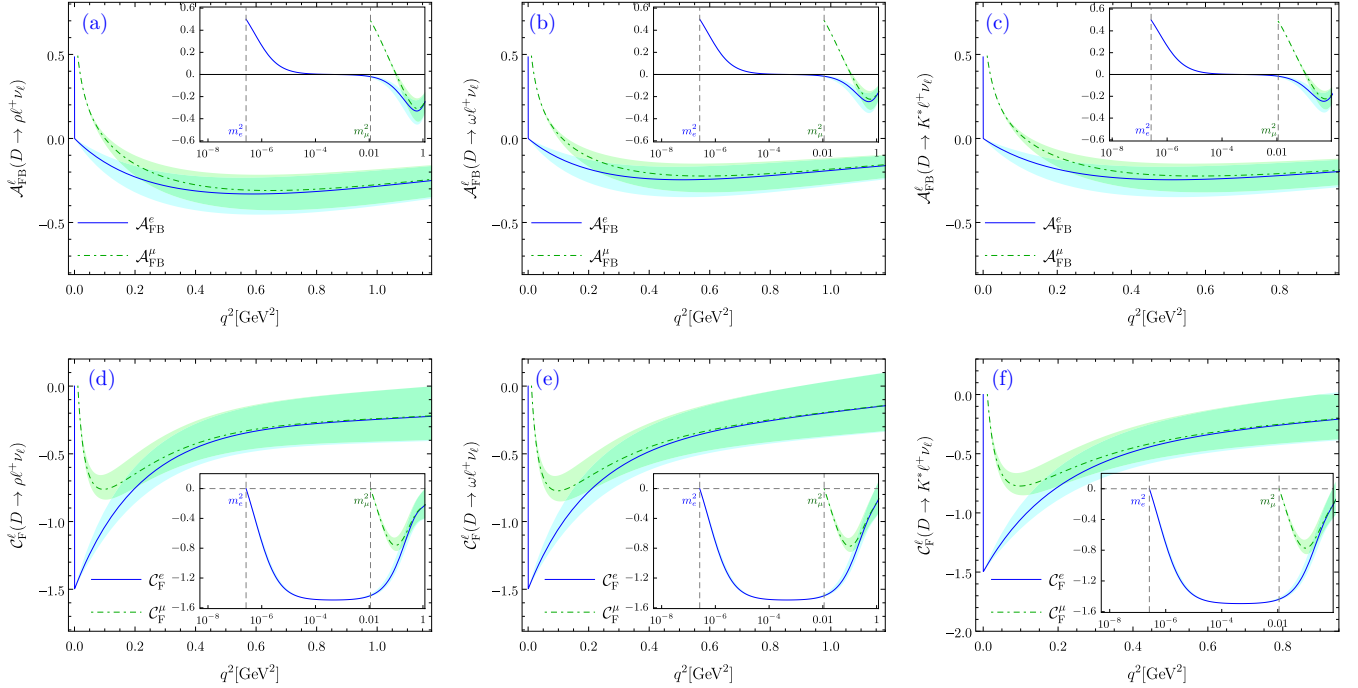
FIG. 5. Forward-backward asymmetry $\mathcal{A}_{\mathrm{FB}}^{\ell}(q^2)$ and the lepton-side $\mathcal{C}_{\mathrm{F}}^{\ell}(q^2)$ convexity parameter as a function of q^2 for $D \to V(\rho, \omega, K^*)\ell^+\nu_\ell$. The lines are their central values, and the shaded bands are their errors. The meaning of the corresponding representations are the same as in Fig. 4.

rapidly, then decrease to the minimum value slowly, and, finally, almost level off. $\mathcal{A}_{\mathrm{FB}}^{e(\mu)} = 0$ is around $q^2 = 0.1\,\mathrm{GeV}^2$ ($q^2 = 10^{-4}\,\mathrm{GeV}^2$), and all $\mathcal{A}_{\mathrm{FB,max}}^{\ell} \approx 0.5$ are shown in the small inset at $q^2 = m_e^2$ ($q^2 = m_\mu^2$). All of these phenomena can be derived from the forward-backward asymmetry analytic expression (9). Therefore, one should be especially careful when dealing with $\mathcal{A}_{\mathrm{FB}}^{\ell}$ in the small-q^2 region, while the forward-backward asymmetry will be easier to study in the large-q^2 region due to the relatively stable value of the $\mathcal{A}_{\mathrm{FB}}^{\ell}$.

(ii) For the bottom parts of Fig. 5, we observe that $\mathcal{C}_{\mathrm{F}}^{\ell}(q^2) \lesssim 0$, $\mathcal{C}_{\mathrm{F}}^{\ell}(q_{\min}^2 = m_{e,\mu}^2) = 0$. All $\mathcal{C}_{\mathrm{F}}^{\ell}(q^2)$ decrease sharply and then

increase, and there is a singularity around low q^2, which is shown in the inset with the logarithmic axis.

The mean values of those polarization observations of the three $D \to V$ semileptonic decay channels are calculated by applying Eq. (11) and are listed in Table VI. Our predictions are the same as the CCQM results within the error bars.

IV. SUMMARY

In this paper, $D \to V(\omega, \rho, K^*)$ HFFs $\mathcal{D}_{V,\sigma}$, with $\sigma = 0, 1, 2, t$, were studied by applying the LCSR and taking into

TABLE VI. The mean values for the longitudinal and transverse polarization fraction of the final lepton and vector mesons, forward-backward asymmetry, and the lepton-side convexity parameter for positron and muon modes, where the uncertainties are the square average of all the input parameters.

	$D \to \rho\ell^+\nu_\ell$		$D \to \omega\ell^+\nu_\ell$		$D \to K^*\ell^+\nu_\ell$	
	This work	CCQM [59]	This work	CCQM [59]	This work	CCQM [59]
$\langle P_{\mathrm{L}}^e \rangle$	$+1.000_{-0.209}^{+0.168}$	$+1.00$	$+1.000_{-0.244}^{+0.188}$	$+1.00$	$+1.000_{-0.170}^{+0.136}$	$+1.00$
$\langle P_{\mathrm{L}}^\mu \rangle$	$+0.968_{-0.211}^{+0.170}$	$+0.92$	$+0.969_{-0.245}^{+0.190}$	0.92	$+0.958_{-0.171}^{+0.138}$	$+0.91$
$\langle P_{\mathrm{T}}^e \rangle \times 10^2$	$-0.093_{-0.114}^{+0.026}$	-0.09	$-0.092_{-0.018}^{+0.024}$	-0.09	$-0.106_{-0.019}^{+0.023}$	-0.11
$\langle P_{\mathrm{T}}^\mu \rangle$	$-0.189_{-0.053}^{+0.042}$	-0.13	$-0.186_{-0.037}^{+0.048}$	-0.12	$-0.213_{-0.038}^{+0.046}$	-0.15
$\langle F_{\mathrm{L}}^e \rangle$	$+0.457_{-0.067}^{+0.055}$	$+0.53$	$+0.441_{-0.057}^{+0.045}$	$+0.52$	$+0.472_{-0.042}^{+0.036}$	$+0.54$
$\langle F_{\mathrm{L}}^\mu \rangle$	$+0.461_{-0.065}^{+0.053}$	$+0.51$	$+0.445_{-0.055}^{+0.044}$	$+0.50$	$+0.478_{-0.041}^{+0.035}$	$+0.52$
$\langle \mathcal{A}_{\mathrm{FB}}^e \rangle$	$-0.293_{-0.117}^{+0.094}$	-0.21	$-0.203_{-0.094}^{+0.071}$	-0.21	$-0.208_{-0.066}^{+0.052}$	-0.18
$\langle \mathcal{A}_{\mathrm{FB}}^\mu \rangle$	$-0.279_{-0.113}^{+0.091}$	-0.24	$-0.191_{-0.090}^{+0.068}$	-0.24	$-0.192_{-0.062}^{+0.049}$	-0.21
$\langle \mathcal{C}_{\mathrm{F}}^e \rangle$	$-0.278_{-0.205}^{+0.165}$	-0.44	$-0.242_{-0.222}^{+0.173}$	-0.43	$-0.312_{-0.151}^{+0.123}$	-0.47
$\langle \mathcal{C}_{\mathrm{F}}^\mu \rangle$	$-0.268_{-0.199}^{+0.162}$	-0.36	$-0.233_{-0.216}^{+0.169}$	-0.35	$-0.297_{-0.146}^{+0.119}$	-0.37

account the LCDAs up to twist 4. The resultant LCSRs for the HFFs are arranged according to the twist structure of the final vector meson LCDAs. Those HFFs are extrapolated to the whole physics q^2 region $m_\ell^2 \leqslant q^2 \leqslant (m_D - m_V)^2$, and then we use extrapolated HFF's to investigate the physical observable for the $D \to V(\rho, \omega, K^*)\ell^+\nu_\ell$ semileptonic decays.

The transversal HFFs and their errors increase as q^2 decreases due to the depression effect from the q^2 coefficient, especially for $\mathcal{D}_{V,1,2}(0) = 0(\pm 0)$ with $V = \rho, \omega, K^*$ mesons. This depression effect from the q^2 coefficient will also be reflected in the different transverse decay widths through transversal HFFs, which can be clearly seen from Fig. 3; we also found $1/|V_{cq}|^2 \times d\Gamma_V^{\mathrm{T}}(0) = 0(\pm 0)$ with $V = \rho, \omega, K^*$ mesons. However, this depression effect for the longitudinal part will disappear due to the missing q^2 coefficient. Thus, the transverse differential decay width dominates the small-q^2 region, while the longitudinal differential decay width dominates the large-q^2 region, and the position of the alternating point of the dominant q^2 region is near the midpoint of the whole physically feasible region. In addition, the decay width (transverse, longitudinal, and total decay widths) decreases with the increase of meson mass in the final state, and the differences between the transverse decay width and longitudinal decay width are almost the same for the three decay channels, which can be seen from Table III. With the help of lifetimes $\tau(D^0)$ and $\tau(D^+)$, we calculate the branching ratio and list it in Table V. Our predictions are lower than other theories, but they fit well with BESIII.

We also investigated in detail the polarization observation dependence on the square momentum transfer for $D \to V(\rho, \omega, K^*)\ell^+\nu_\ell$ semileptonic decays with $\ell = e, \mu$, which have a similar shape for different final mesons and the same final lepton. In the small-q^2 region, all those polarization observations have a singularity due to the δ_ℓ factor, which is shown in the small graph with the logarithmic axis, except for $F_{\mathrm{L,T}}^\ell$. With the increase of q^2, all polarization values tend to be more stable; thus, the polarization dependence on q^2 declines. Note that F_{L}^ℓ and F_{T}^ℓ dominate the small-q^2 region and the large-q^2 region, respectively, and the position of the alternating point of the dominant q^2 region is near the center of the whole physically feasible region, which roughly equates to the positions of the dominant alternating points of the transverse

TABLE VII. The moments and couplings of vector meson twist-2, -3, -4 LCDAs; the corresponding scale is $\mu^2 = m_D^2 - m_c^2 \approx 1\,\mathrm{GeV}^2$.

	ρ	ω	K^*
$a_1^\parallel$	0	0	0.19(5)
$a_2^\parallel$	0.18(10)	0.18(10)	0.06(6)
$a_1^\perp$	0	0	0.20(5)
$a_2^\perp$	0.20(10)	0.18(10)	0.04(4)
δ_+	0	0	0.24
δ_-	0	0	-0.24
$\tilde{\delta}_+$	0	0	0.16
$\tilde{\delta}_-$	0	0	-0.16

and longitudinal differential decay widths. We also calculated the corresponding average values and listed them in Table VI; they coincide with CCQM within the error bars.

APPENDIX

In order to get accurate HFFs results within the LCSR approach for the semileptonic decay processes $D \to V(\rho, \omega, K^*)\ell^+\nu_\ell$ and to make a comparison with other theoretical and experimental results, we take the twist-2, -3, -4 LCDAs given by Ball and Braun [61] used by many theoretical predictions. The two-particle LCDAs for twist 3 has the following form:

$$\psi_{3;V}^\perp(u) = 6u\bar{u}\left[1 + a_1^\parallel \xi + \left\{\frac{1}{4}a_2^\parallel + \frac{5}{3}\zeta_3\left(1 - \frac{3}{16}\omega_3^A + \frac{9}{16}\omega_3^V\right)\right\}(5\xi^2 - 1)\right] + 6\tilde{\delta}_+(3u\bar{u} + \bar{u}\ln\bar{u} + u\ln u)$$
$$+ 6\tilde{\delta}_-(\bar{u}\ln\bar{u} - u\ln u), \tag{A1}$$

$$\phi_{3;V}^\perp(u) = \frac{3}{4}(1 + \xi^2) + a_1^\parallel\frac{3}{2}\xi^3 + \left(\frac{3}{7}a_2^\parallel + 5\zeta_3\right)(3\xi^2 - 1) + \left[\frac{9}{112}a_2^\parallel + \frac{15}{64}\zeta_3\left(3\omega_3^V - \omega_3^A\right)\right](3 - 30\xi^2 + 35\xi^4)$$
$$+ \frac{3}{2}\tilde{\delta}_+(2 + \ln u + \ln\bar{u}) + \frac{3}{2}\tilde{\delta}_-(2\xi + \ln\bar{u} - \ln u), \tag{A2}$$

$$\psi_{3;V}^\parallel(u) = 6u\bar{u}\left[1 + a_1^\perp\xi + \left(\frac{1}{4}a_2^\perp + \frac{5}{8}\zeta_3\omega_3^T\right)(5\xi^2 - 1)\right] + 3\delta_+(3u\bar{u} + \bar{u}\ln\bar{u} + u\ln u) + 3\delta_-(\bar{u}\ln\bar{u} - u\ln u), \tag{A3}$$

$$\phi_{3;V}^\parallel(u) = 3\xi^2 + \frac{3}{2}a_1^\perp\xi(3\xi^2 - 1) + \frac{3}{2}a_2^\perp\xi^2(5\xi^2 - 3) + \frac{15}{16}\zeta_3\omega_3^T(3 - 30\xi^2 + 35\xi^4) + \frac{3}{2}\delta_+\left(1 + \xi\ln\frac{\bar{u}}{u}\right)$$
$$+ \frac{3}{2}\delta_-\xi(2 + \ln u + \ln\bar{u}). \tag{A4}$$

The two-particle LCDAs for twist-4 can be written as

$$\psi_{4;V}^{\perp}(u) = 6u(1-u) + 5\big[\zeta_4^{\mathrm{T}} + \tilde{\zeta}_4^{\mathrm{T}}\big](1 - 3\xi^2), \tag{A5}$$

$$\phi_{4;V}^{\perp}(u) = 30u^2(1-u)^2\big[\tfrac{2}{5} + \tfrac{4}{3}\zeta_4^{\mathrm{T}} - \tfrac{8}{3}\tilde{\zeta}_4^{\mathrm{T}}\big], \tag{A6}$$

$$\phi_{4;V}^{\parallel}(u) = \big[\tfrac{4}{5} + \tfrac{20}{9}\zeta_4 + \tfrac{8}{9}\zeta_3\big]30u^2\bar{u}^2, \tag{A7}$$

$$\psi_{4;V}^{\parallel}(u) = 6u\bar{u} + \big[\tfrac{10}{3}\zeta_4 - \tfrac{20}{3}\zeta_3\big](1 - 3\xi^2), \tag{A8}$$

$$C_V(u) = \big[\tfrac{3}{2} + \tfrac{10}{3}\zeta_4 + \tfrac{10}{3}\zeta_3\big]u^2\bar{u}^2. \tag{A9}$$

The values of the moments and coupling constants of the vector meson twist-2, -3, -4 LCDAs are listed in Table VII. At the scale $\mu^2 = m_D^2 - m_c^2 \approx 1\,\mathrm{GeV}^2$, the couplings for twist-3 and twist-4 LCDAs are

$$\zeta_3 = 0.032, \quad \omega_3^A = -2.1, \quad \omega_3^V = 3.8, \quad \omega_3^T = 7.0,$$

$$\zeta_4 = 0.15, \quad \zeta_4^T = 0.10, \quad \tilde{\zeta}_4^T = -0.10. \tag{A10}$$

[1] J. Charles *et al.* [CKMfitter Group], CP violation and the CKM matrix: Assessing the impact of the asymmetric *B* factories, Eur. Phys. J. C **41**, 1 (2005).

[2] A. Poluektov *et al.* (Belle Collaboration), Evidence for direct CP violation in the decay $B^{\pm} \to D^{(*)}K^{\pm}, D \to K_s^0\pi + \pi-$ and measurement of the CKM phase ϕ_3, Phys. Rev. D **81**, 112002 (2010).

[3] M. Bona, A. Contu, G. Fedi, and M. J. Morello, CKM matrix and *CP* violation in charm and beauty, PoS **(PP@LHC2016)** 009 (2016).

[4] K. Abe *et al.* (T2K Collaboration), Search for *CP* Violation in Neutrino and Antineutrino Oscillations by the T2K Experiment with 2.2×10^{21} Protons on Target, Phys. Rev. Lett. **121**, 171802 (2018).

[5] R. Aaij *et al.* (LHCb Collaboration), Observation of *CP* Violation in Charm Decays, Phys. Rev. Lett. **122**, 211803 (2019).

[6] S. Funatsu, H. Hatanaka, Y. Hosotani, Y. Orikasa, and N. Yamatsu, CKM matrix and FCNC suppression in SO(5) × U(1) × SU(3) gauge-Higgs unification, Phys. Rev. D **101**, 055016 (2020).

[7] P. K. Resmi *et al.* (Belle Collaboration), First measurement of the CKM angle ϕ_3 with $B^{\pm} \to D(K_S^0\pi^+\pi^-\pi^0)K^{\pm}$ decays, J. High Energy Phys. 10 (2019) 178.

[8] B. Belfatto, R. Beradze, and Z. Berezhiani, The CKM unitarity problem: A trace of new physics at the TeV scale? Eur. Phys. J. C **80**, 149 (2020).

[9] J. Drobnak, S. Fajfer, and J. F. Kamenik, Signatures of NP models in top FCNC decay $t \to c(u)\ell^+\ell^-$, J. High Energy Phys. 03 (2009) 077.

[10] F. J. Botella, G. C. Branco, A. Carmona, M. Nebot, L. Pedro, and M. N. Rebelo, Physical constraints on a class of two-Higgs doublet models with FCNC at tree level, J. High Energy Phys. 07 (2014) 078.

[11] C. S. Kim, Y. W. Yoon, and X.-B. Yuan, Exploring top quark FCNC within 2HDM type III in association with flavor physics, J. High Energy Phys. 12 (2015) 038.

[12] D. Melikhov, A. Kozachuk, and N. Nikitin, Rare FCNC radiative leptonic $B_{s,d} \to \gamma\ell^+\ell^-$ decays in the SM, PoS **(Confinement2018)** 274 (2019).

[13] K. Y. Oyulmaz, A. Senol, H. Denizli, and O. Cakir, Top quark anomalous FCNC production via *tqg* couplings at FCC-hh, Phys. Rev. D **99**, 115023 (2019).

[14] M. Ablikim *et al.* (BESIII Collaboration), Observation of the Singly Cabibbo-Suppressed Decay $D^+ \to \omega\pi^+$ and Evidence for $D^0 \to \omega\pi^0$, Phys. Rev. Lett. **116**, 082001 (2016).

[15] M. Ablikim *et al.* (BES-III Collaboration), Measurement of the absolute branching fraction of $D^+ \to \bar{K}^0e^+\nu_e$ via $\bar{K}^0 \to \pi^0\pi^0$, Chin. Phys. C **40**, 113001 (2016).

[16] M. Ablikim *et al.* (BESIII Collaboration), Measurement of the form factors in the decay $D^+ \to \omega e^+\nu_e$ and search for the decay $D^+ \to \phi e^+\nu_e$, Phys. Rev. D **92**, 071101 (2015).

[17] P. Naik *et al.* (CLEO Collaboration), Measurement of the pseudoscalar decay constant f_{D_s} using $D_s^+ \to \tau^+\nu, \tau^+ \to \rho^+\bar{\nu}$ decays, Phys. Rev. D **80**, 112004 (2009).

[18] L. Martin *et al.* (CLEO Collaboration), Search for the decay $D_s^+ \to \omega e^+\nu$, Phys. Rev. D **84**, 012005 (2011).

[19] P. U. E. Onyisi *et al.* (CLEO Collaboration), Improved measurement of absolute hadronic branching fractions of the D_s^+ meson, Phys. Rev. D **88**, 032009 (2013).

[20] T. E. Coan *et al.* (CLEO Collaboration), Absolute Branching Fraction Measurements of Exclusive D^0 Semileptonic Decays, Phys. Rev. Lett. **95**, 181802 (2005).

[21] R. A. Briere *et al.* (CLEO Collaboration), Analysis of $D^+ \to K^-\pi^+e^+\nu_e$ and $D^+ \to K^-\pi^+\mu^+\nu_\mu$ semileptonic decays, Phys. Rev. D **81**, 112001 (2010).

[22] S. Dobbs *et al.* (CLEO Collaboration), First Measurement of the Form Factors in the Decays $D^0 \to \rho^-e^+\nu_e$ and $D^+ \to \rho^0e^+\nu_e$, Phys. Rev. Lett. **110**, 131802 (2013).

[23] M. Ablikim *et al.* (BESIII Collaboration), First Observation of $D^+ \to f_0(500)e^+\nu_e$ and Improved Measurements of $D \to \rho e^+\nu_e$, Phys. Rev. Lett. **122**, 062001 (2019).

[24] M. Ablikim *et al.* (BESIII Collaboration), Study of the decay $D^0 \to \bar{K}^0\pi^-e^+\nu_e$, Phys. Rev. D **99**, 011103 (2019).

[25] M. Ablikim *et al.* (BESIII Collaboration), Observation of the semimuonic decay $D^+ \to \omega\mu^+\nu_\mu$, Phys. Rev. D **101**, 072005 (2020).

[26] Y. Grossman and D. Pirjol, Extracting and using photon polarization information in radiative B decays, J. High Energy Phys. 06 (2000) 029.

[27] M. Gronau, Y. Grossman, D. Pirjol, and A. Ryd, Measuring the Photon Polarization in $B \to K\pi\pi\gamma$, Phys. Rev. Lett. **88**, 051802 (2002).

[28] F. Kruger and J. Matias, Probing new physics via the transverse amplitudes of $B^0 \to K^{*0}(\to K^-\pi^+)\ell^+\ell^-$ at large recoil, Phys. Rev. D **71**, 094009 (2005).

[29] E. Kou, A. Le Yaouanc, and A. Tayduganov, Determining the photon polarization of the $b \to s\gamma$ using the $B \to K_1(1270)\gamma \to (K\pi\pi)\gamma$ decay, Phys. Rev. D **83**, 094007 (2011).

[30] S. Wehle, Angular Analysis of $B \to K^*\ell\ell$ and Search for $B^+ \to K^+\tau\tau$ at the Belle Experiment, Ph.D. thesis, University Hamburg, 2016.

[31] W. Cheng, X. G. Wu, and H. B. Fu, Reconsideration of the $B \to K^*$ transition form factors within the QCD light-cone sum rules, Phys. Rev. D **95**, 094023 (2017).

[32] H. B. Fu, X. G. Wu, W. Cheng, T. Zhong, and Z. Sun, Asymmetries of the $B \to K^*\mu^+\mu^-$ decay and the search of new physics beyond the standard model, Phys. Rev. D **97**, 055037 (2018).

[33] R. Y. Zhou, L. Guo, H. B. Fu, W. Cheng, and X. G. Wu, The $B \to \pi\ell\nu_\ell$ semileptonic decay within the LCSR approach under heavy quark effective field theory, Chin. Phys. C **44**, 013101 (2020).

[34] W. Wang, F.-S. Yu, and Z.-X. Zhao, Novel Method to Reliably Determine the Photon Helicity in $B \to K_1\gamma$, Phys. Rev. Lett. **125**, 051802 (2020).

[35] L. M. García Martín, B. Jashal, F. Martínez Vidal, A. Oyanguren, S. Roy, R. Sain, and R. Sinha, Radiative b-baryon decays to measure the photon and b-baryon polarization, Eur. Phys. J. C **79**, 634 (2019).

[36] V. M. Braun, Light cone sum rules, arXiv:hep-ph/9801222.

[37] T. Huang and Z. H. Li, $B \to K^*\gamma$ in the light cone QCD sum rule, Phys. Rev. D **57**, 1993 (1998).

[38] T. Huang, Z. H. Li, and X. Y. Wu, Improved approach to the heavy to light form-factors in the light cone QCD sum rules, Phys. Rev. D **63**, 094001 (2001).

[39] X. G. Wu, T. Huang, and Z. Y. Fang, $SU_f(3)$ symmetry breaking effects of the $B \to K$ transition form-factor in the QCD light-cone sum rules, Phys. Rev. D **77**, 074001 (2008).

[40] S. Momeni, R. Khosravi, and F. Falahati, Flavor changing neutral current transition of $B \to a_1$ with light-cone sum rules, Phys. Rev. D **95**, 016009 (2017).

[41] Y. M. Wang, Y. B. Wei, Y. L. Shen, and C. D. Lü, Perturbative corrections to $B \to D$ form factors in QCD, J. High Energy Phys. 06 (2017) 062.

[42] X. D. Cheng, H. B. Li, B. Wei, Y. G. Xu, and M. Z. Yang, Study of $D \to a_0(980)e^+\nu_e$ decay in the light-cone sum rules approach, Phys. Rev. D **96**, 033002 (2017).

[43] H. B. Fu, L. Zeng, R. Lü, W. Cheng, and X. G. Wu, The $D \to \rho$ semileptonic and radiative decays within the light-cone sum rules, Eur. Phys. J. C **80**, 194 (2020).

[44] J. Gao, C. D. Lü, Y. L. Shen, Y. M. Wang, and Y. B. Wei, Precision calculations of $B \to V$ form factors in QCD, Phys. Rev. D **101**, 074035 (2020).

[45] S. Momeni and R. Khosravi, Semileptonic $D_{(s)} \to A\ell^+\nu$ and nonleptonic $D \to K_1(1270, 1400)\pi$ decays in LCSR, J. Phys. G **46**, 105006 (2019).

[46] I. I. Balitsky, V. M. Braun, and A. V. Kolesnichenko, Radiative decay $\sigma^+ \to p\gamma$ in quantum chromodynamics, Nucl. Phys. B **312**, 509 (1989).

[47] V. L. Chernyak and I. R. Zhitnitsky, B meson exclusive decays into baryons, Nucl. Phys. B **345**, 137 (1990).

[48] V. M. Belyaev, A. Khodjamirian, and R. Ruckl, QCD calculation of the $B \to \pi, K$ form-factors, Z. Phys. C **60**, 349 (1993).

[49] P. Ball and V. M. Braun, Use and misuse of QCD sum rules in heavy to light transitions: The decay $B \to \rho e\nu$ reexamined, Phys. Rev. D **55**, 5561 (1997).

[50] P. Ball and R. Zwicky, $B_{(ds)} \to \rho, \omega, K^*, \phi$ decay form factors from light-cone sum rules revisited, Phys. Rev. D **71**, 014029 (2005).

[51] S. Fajfer and J. F. Kamenik, Charm meson resonances and $D \to V$ semileptonic form factors, Phys. Rev. D **72**, 034029 (2005).

[52] W. Wang and Y. L. Shen, $D_s \to K, K^*, \phi$ form factors in the covariant light-front approach and exclusive D_s decays, Phys. Rev. D **78**, 054002 (2008).

[53] R. N. Faustov, V. O. Galkin, and X. W. Kang, Semileptonic decays of D and D_s mesons in the relativistic quark model, Phys. Rev. D **101**, 013004 (2020).

[54] W. Cheng, X. G. Wu, R. Y. Zhou, and H. B. Fu, The $B \to \rho$ helicity form factors within the QCD light-cone sum rules, Phys. Rev. D **98**, 096013 (2018).

[55] A. Bharucha, T. Feldmann, and M. Wick, Theoretical and phenomenological constraints on form factors for radiative and semi-leptonic B-meson decays, J. High Energy Phys. 09 (2010) 090.

[56] H. B. Fu, W. Cheng, R. Y. Zhou, and L. Zeng, $D \to P(\pi, K)$ helicity form factors within LCSR, Chin. Phys. C **44**, 113103 (2020).

[57] D. Leljak, B. Melic, and M. Patra, On lepton flavour universality in semileptonic $B_c \to \eta_c, J/\psi$ decays, J. High Energy Phys. 05 (2019) 094.

[58] M. Tanabashi *et al.* (Particle Data Group), Review of particle physics, Phys. Rev. D **98**, 030001 (2018).

[59] M. A. Ivanov, J. G. Körner, J. N. Pandya, P. Santorelli, N. R. Soni, and C. T. Tran, Exclusive semileptonic decays of D and D_s mesons in the covariant confining quark model, Front. Phys. **14**, 64401 (2019).

[60] H. B. Fu, X. G. Wu, H. Y. Han, and Y. Ma, $B \to \rho$ transition form factors and the ρ meson transverse leading-twist distribution amplitude, J. Phys. G **42**, 055002 (2015).

[61] P. Ball and V. M. Braun, Exclusive semileptonic and rare B meson decays in QCD, Phys. Rev. D **58**, 094016 (1998).

[62] D. Melikhov and B. Stech, Weak form factors for heavy meson decays: An update, Phys. Rev. D **62**, 014006 (2000).

[63] W. Y. Wang, Y. L. Wu, and M. Zhong, Heavy to light meson exclusive semileptonic decays in effective field theory of heavy quarks, Phys. Rev. D **67**, 014024 (2003).

[64] P. Ball, V. M. Braun, and H. G. Dosch, Form factors of semileptonic D decays from QCD sum rules, Phys. Rev. D **44**, 3567 (1991).

[65] C. R. Allton *et al.* (APE Collaboration), Lattice calculation of D and B meson semileptonic decays using the clover action at $\beta = 6.0$ on APE, Phys. Lett. B **345**, 513 (1995).

[66] H. Y. Cheng and X. W. Kang, Branching fractions of semileptonic D and D_s decays from the covariant light-front quark model, Eur. Phys. J. C **77**, 587 (2017).

[67] T. Sekihara and E. Oset, Investigating the nature of light scalar mesons with semileptonic decays of D mesons, Phys. Rev. D **92**, 054038 (2015).

[68] Y. L. Wu, M. Zhong, and Y. B. Zuo, $B_{(s)}, D_{(s)} \rightarrow \pi, K, \eta, \rho, K^*, \omega, \phi$ transition form factors and decay rates with extraction of the CKM parameters $|V_{ub}|, |V_{cs}|, |V_{cd}|$, Int. J. Mod. Phys. A **21**, 6125 (2006).